

SATURATING STIFFNESS CONTROL OF ROBOT MANIPULATORS WITH BOUNDED INPUTS

MARÍA DEL CARMEN RODRÍGUEZ-LIÑÁN^a, MARCO MENDOZA^{b,*}, ISELA BONILLA^b,
CÉSAR A. CHÁVEZ-OLIVARES^c

^aCONACYT—Ensenada Institute of Technology
Boulevard Tecnológico No. 150, Col. Ex Ejido Chapultepec, Ensenada, Baja California, 22780 Mexico
e-mail: macaroli270@yahoo.com.mx

^bFaculty of Sciences
Autonomous University of San Luis Potosí, Av. Salvador Nava S/N, San Luis Potosí, SLP, 78290 Mexico
e-mail: {marco.mendoza, isela.bonilla}@uaslp.mx

^cRobotics Engineering Department
Autonomous University of Aguascalientes, Prol. Mahatma Gandhi 6601, Aguascalientes, Ags., 20392 Mexico
e-mail: cesar.chavez@edu.uaa.mx

A saturating stiffness control scheme for robot manipulators with bounded torque inputs is proposed. The control law is assumed to be a PD-type controller, and the corresponding Lyapunov stability analysis of the closed-loop equilibrium point is presented. The interaction between the robot manipulator and the environment is modeled as spring-like contact forces. The proper behavior of the closed-loop system is validated using a three degree-of-freedom robotic arm.

Keywords: bounded inputs, robot manipulator, saturation, stiffness control.

1. Introduction

Nowadays, robotic systems are very popular in various types of applications (Djebrani *et al.*, 2012; Duleba and Opałka, 2013; Yarza *et al.*, 2013; Belter *et al.*, 2016). The presence of robots in the industry is one of the best known of, but other areas like medical services are taking more and more advantage of these systems. Applications like rehabilitation robotics (therapies, home assistance, orthopedics, etc.) and surgery are worth mentioning here (Dario *et al.*, 1994).

Regardless of the field, robotic tasks can be divided into two categories, depending on the robot–environment interaction, i.e., unconstrained or constrained motions. The former refers to applications where there is no interaction with the environment. In the latter, the motion of the robot is restricted by some interaction with the medium. In constrained motion tasks, there is an ever present mechanical coupling between the robot and its surroundings; moreover, this interaction could change

over time, which implies that the interaction forces cannot be disregarded (Hogan, 1985).

To deal with constrained motion systems, two methods have been proposed. The first one, known as the direct method, uses force-feedback to specify the desired interaction force (Volpe and Khosla, 1993). The second strategy is indirect force control, whose main scheme is impedance control, as proposed by Hogan (1985); this approach relates the position errors to the interaction forces. The interaction between the end-effector and the environment is then regulated by modifying the system's mechanical impedance. Impedance control has triggered off a number of developments for interaction control. These include, for instance, a Lyapunov-based approach (Mendoza *et al.*, 2012), model predictive impedance control (Falaki and Towhidkhah, 2012), model-free impedance control (Li *et al.*, 2011) or intelligent control like neural networks (Dehghani *et al.*, 2010; Modares *et al.*, 2016), fuzzy logic (Deneve *et al.*, 2008; Akdoğan and Adli, 2011; Ju *et al.*, 2005), or a combination of

*Corresponding author

both (Kiguchi *et al.*, 2007; Xu *et al.*, 2011), as well as stiffness control in the task-space as in the work of Chávez-Olivares *et al.* (2015), where some case studies of different stiffness regulators are proposed and the corresponding Lyapunov's stability analysis is presented.

Impedance control and stiffness control are both forms of indirect force control. In order to achieve the *desired dynamic behavior*, impedance control intends to regulate mechanical impedance via force feedback (Spong *et al.*, 2005), where a dynamic model-based compensation control scheme leads to task-space closed-loop dynamics given by

$$\ddot{\mathbf{x}} = \ddot{\mathbf{x}}_d - \mathbf{M}_d^{-1}(\mathbf{B}_d \dot{\mathbf{e}} + \mathbf{K}_d \mathbf{e} + \mathbf{f}),$$

where \mathbf{M}_d , \mathbf{B}_d and \mathbf{K}_d are the desired inertia, damping and stiffness matrices, respectively, \mathbf{e} denotes the tracking error and \mathbf{f} is the measured contact force. On the other hand, the objective of stiffness control is to regulate robot stiffness by achieving the *desired static behavior* of the interaction. When robot manipulators are used for force control applications, where the interaction with the environment is critical, a stiff manipulator makes the task harder to achieve. By controlling manipulator stiffness the control objective is more easily attained (Siciliano and Villani, 2012). In this case, it is possible to construct a PD-type controller with gravity compensation of the form

$$\boldsymbol{\tau} = \mathbf{J}^T(\mathbf{q})[-\mathbf{K}_v \dot{\bar{\mathbf{x}}} + \mathbf{K}_p \bar{\mathbf{x}}] + \mathbf{g}(\mathbf{q}),$$

where \mathbf{K}_v is a derivative gain matrix, \mathbf{K}_p is a proportional gain matrix, $\bar{\mathbf{x}} = \mathbf{x}_d - \mathbf{x}$, which is the difference between the desired and the current end-effector position (Kurfess, 2004).

In real systems, saturation is a nonlinearity that always affects their performance. It is due to intrinsic limitations of actuators. As such, every controller design must contemplate the existence of constraints if one wants to implement it in real life. Ignoring this inevitable nonlinearity may lead to an undesired behavior of the system.

In the literature, there are several works that analyze robotic systems with bounded inputs (see Kelly *et al.*, 2005), such as PD with gravity compensation, like feedback controllers with saturating proportional (SP) or saturating derivative (SD) (Kelly *et al.*, 1997; Santibáñez and Kelly, 1996; Santibáñez *et al.*, 1998). These solutions have been proposed assuming specific saturation functions. Alternatively, PD-type controllers with generalized saturation nonlinearities were also developed (see, e.g., Zavala-Río and Santibáñez, 2006; 2007). Aguiñaga-Ruiz *et al.* (2009) propose a tracking control scheme with static feedback to globally stabilize bounded input manipulators. Also, global adaptive regulators for bounded input systems and without a saturation avoidance restriction were developed; for example, in

the work of López-Araujo *et al.* (2013a), an SP-SD algorithm with gravity compensation is proposed, and in another paper the authors present an output feedback regulator without velocity dependence (López-Araujo *et al.*, 2013b). They also use generalized saturation functions to design an adaptive controller for global control of robot manipulators with saturated inputs (López-Araujo *et al.*, 2015). Caverly *et al.* (2014; 2016) propose other PD-type controllers for flexible-joints robotic manipulators while avoiding actuator saturation, and where Gibbs parameterization and a Hammerstein strictly positive real angular rate control term are employed. Recently, saturating PID-type regulators were proposed by Mendoza *et al.* (2015a; 2015b), resulting in the global stability of the equilibrium point of the closed-loop system and with a simple tuning of the controller's parameters.

Additionally, a first step in addressing the problem of interaction control for manipulators with bounded inputs was presented by He *et al.* (2016). Specifically, a neural-network based adaptive impedance control was developed to solve the robot–environment interaction problem. Both full state and output feedback controllers were considered, by using an auxiliary signal to handle the saturation effect of actuators; however, the structure of the control laws does not ensure that the generation of bounded control signals will avoid the actuator saturation.

To our knowledge, in the literature there are no works where constrained–motion controllers (which generate bounded control signals to avoid saturation) for robot manipulators, with bounded torque inputs, and their corresponding stability analyses are presented. In this paper, we present the stability analysis in Lyapunov's sense for a novel saturating stiffness-control structure of robot manipulators. It is assumed that the control structure has a generalized form of a PD-type controller, and that the interaction with the environment can be modeled as a spring-like elastic force. The performance of the saturating controller is tested on a three degree-of-freedom robot manipulator interacting with a rigid work surface.

This paper is organized as follows. Section 2 includes the notation and definitions used in this work. In Section 3, the dynamical model of the robot is presented. The saturating stiffness-control structure proposed is described in Section 4. Section 5 contains the results of two tests for the robot–environment interaction. Finally, conclusions to the paper are presented in Section 6.

2. Notation and definitions

Let $\mathbf{A} \in \mathbb{R}^{n \times m}$ and $\mathbf{x} \in \mathbb{R}^n$. \mathbf{A}_i is the i -th row vector of \mathbf{A} , A_{ij} represents the element of \mathbf{A} pertaining to the i -th row and j -th column of \mathbf{A} ; x_i denotes the i -th element of \mathbf{x} . The origin of \mathbb{R}^n is represented by $\mathbf{0}^n$ and the identity

matrix of dimension $n \times n$ is written as \mathbf{I}^n .

The largest eigenvalue of \mathbf{A} is denoted by $\lambda_{\max}\{\mathbf{A}\}$. The Euclidean norm of vector \mathbf{x} is given as $\|\mathbf{x}\| = \sqrt{\mathbf{x}^T \mathbf{x}}$, while the norm of matrix \mathbf{A} is defined as $\|\mathbf{A}\| = \sqrt{\lambda_{\max}\{\mathbf{A}^T \mathbf{A}\}}$.

Consider a continuously differentiable scalar function $\zeta : \mathbb{R} \mapsto \mathbb{R}$ and a locally Lipschitz, continuous, scalar function $\phi : \mathbb{R} \mapsto \mathbb{R}$, such that $\zeta(0) = \phi(0) = 0$. The derivative with respect to their argument is denoted by

$$\zeta'(\varsigma) = \frac{d\zeta}{d\varsigma}(\varsigma).$$

The upper right derivative of ϕ is defined as

$$D^+ \phi(\varsigma) = \limsup_{h \rightarrow 0^+} \frac{\phi(\varsigma + h) - \phi(\varsigma)}{h}.$$

Thus,

$$\phi(\varsigma) = \int_0^\varsigma D^+ \phi(r) dr,$$

and (cf. Khalil, 2002)

$$(\zeta \circ \phi)(\varsigma) = \zeta(\phi(\varsigma)) = \int_0^\varsigma \zeta'(\phi(r)) D^+ \phi(r) dr.$$

Next, a generalized saturation function is defined as in the work of Mendoza *et al.* (2015a). A non-decreasing, Lipschitz continuous function $\sigma : \mathbb{R} \mapsto \mathbb{R}$ is a generalized saturation one, bounded by $M > 0$, in the following cases:

- $\varsigma \sigma(\varsigma) > 0, \forall \varsigma \neq 0$.
- $|\sigma(\varsigma)| \leq M, \forall \varsigma \in \mathbb{R}$.
- If, in addition, $\sigma(\varsigma) = \varsigma$ when $|\varsigma| \leq L$, for some $0 < L \leq M$, it is said that σ is a linear saturation function for (L, M) .

A generalized saturation function σ satisfies the properties listed below, proved by López-Araujo *et al.* (2013a). For a constant $k > 0$, the following holds:

- $\lim_{|\varsigma| \rightarrow \infty} D^+ \sigma(\varsigma) = 0$.
- $\exists \sigma'_M \in (0, \infty) : 0 \leq D^+ \sigma(\varsigma) \leq \sigma'_M, \forall \varsigma \in \mathbb{R}$.
- $\frac{\sigma^2(k\varsigma)}{2k\sigma'_M} \leq \int_0^\varsigma \sigma(kr) dr \leq \frac{k\sigma'_M \varsigma^2}{2}, \forall \varsigma \in \mathbb{R}$.
- $\int_0^\varsigma \sigma(kr) dr > 0, \forall \varsigma \neq 0$.
- $\int_0^\varsigma \sigma(kr) dr \rightarrow \infty$ as $\varsigma \rightarrow \infty$.
- If σ is strictly increasing, then
 - $\varsigma[\sigma(\varsigma + \eta) - \sigma(\eta)] > 0, \forall \varsigma \neq 0, \forall \eta \in \mathbb{R}$;
 - $\bar{\sigma}(\varsigma) = \sigma(\varsigma + a) - \sigma(a)$ is generalized saturation function, strictly bounded by $\bar{M} = M + |\sigma(a)|$, for any constant $a \in \mathbb{R}$.

- If σ is a linear saturation for (L, M) , then, for any continuous function $\nu : \mathbb{R} \mapsto \mathbb{R}$, such that $|\nu(\eta)| < L, \forall \eta \in \mathbb{R}$, we have $\varsigma[\sigma(\varsigma + \nu(\eta)) - \sigma(\nu(\eta))] > 0$, for all $\varsigma \neq 0$ and for all $\eta \in \mathbb{R}$.

3. Dynamic model of a robot manipulator

The dynamic model of a robot manipulator of n degrees of freedom (DOFs), interacting with the environment in a p -dimensional task-space, can be described as

$$\mathbf{M}(\mathbf{q})\ddot{\mathbf{q}} + \mathbf{C}(\mathbf{q}, \dot{\mathbf{q}})\dot{\mathbf{q}} + \mathbf{F}\dot{\mathbf{q}} + \mathbf{g}(\mathbf{q}) = \tau - \mathbf{J}^T(\mathbf{q})\mathbf{f}_e, \quad (1)$$

where $\mathbf{q} \in \mathbb{R}^n$ is the joint displacement vector, $\dot{\mathbf{q}} \in \mathbb{R}^n$ is the joint velocity vector, $\ddot{\mathbf{q}} \in \mathbb{R}^n$ is the joint acceleration vector, $\mathbf{M}(\mathbf{q}) \in \mathbb{R}^{n \times n}$ is the (symmetric and positive definite) inertia matrix, $\mathbf{C}(\mathbf{q}, \dot{\mathbf{q}})\dot{\mathbf{q}} \in \mathbb{R}^n$ is the vector of centripetal and Coriolis torques, $\mathbf{g}(\mathbf{q}) \in \mathbb{R}^n$ is the vector of gravitational torques, and \mathbf{F} is the (diagonal and positive definite) viscous friction matrix. The vector of control torques is represented by $\tau \in \mathbb{R}^n$, $\mathbf{J}(\mathbf{q}) \in \mathbb{R}^{p \times n}$ represents the Jacobian matrix of the manipulator, and the external interaction forces are given by $\mathbf{f}_e \in \mathbb{R}^p$. The following properties of the dynamic model are very useful for further analysis (Kelly *et al.*, 2005).

Property 1. The gravity torque term $\mathbf{g}(\mathbf{q})$ is a bounded vector function.¹ Equivalently, the elements of the vector of gravitational torques, $g_i(\mathbf{q}), i = 1, \dots, n$, satisfy $|g_i(\mathbf{q})| \leq B_{gi}, \forall \mathbf{q} \in \mathbb{R}^n$, for some positive constant B_{gi} .

Property 2. Consider the vector of external interaction torques $\mathbf{J}^T(\mathbf{q})\mathbf{f}_e$, let f_{eMj} represent an upper bound of f_{ej} such that $f_{ej} \leq f_{eMj}$, and let $\mathbf{f}_{eM} \triangleq (f_{eM1}, \dots, f_{eMp})^T$ and $\mathbf{F}_e \triangleq [-f_{eM1}, f_{eM1}] \times \dots \times [-f_{eMp}, f_{eMp}]$. For robot manipulators having only revolute joints, there exist positive constants B_{Jij}, B_{Ji} , and B_J such that $|J_{ij}^T(\mathbf{q})| \leq B_{Jij}, \|\mathbf{J}_i^T(\mathbf{q})\| \leq B_{Ji}$, and $\|\mathbf{J}^T(\mathbf{q})\| \leq B_J, \forall \mathbf{q} \in \mathbb{R}^n, i = 1, \dots, n, j = 1, \dots, p$. Furthermore, there exist positive constants B_{Jfi} such that $|\mathbf{J}_i^T(\mathbf{q})\mathbf{f}_e| \leq B_{Jfi}, i = 1, \dots, n, \forall \mathbf{q} \in \mathbb{R}^n, \forall \mathbf{f}_e \in \mathbf{F}_e$.

Suppose that each component of vector τ (namely, τ_i) is bounded by a saturation limit $T_i > 0$; that is, $|\tau_i| \leq T_i$, with $i = 1, \dots, n$. Then, if u_i represents the control signal to the i -th degree of freedom, we have the following relationship:

$$\tau_i = T_i \text{sat}\left(\frac{u_i}{T_i}\right), \quad (2)$$

where $\text{sat}(\cdot)$ is the standard saturation function, $\text{sat}(\varsigma) = \text{sign}(\varsigma) \min\{|\varsigma|, 1\}$ (Mendoza *et al.*, 2015a).

The relationship between the control forces applied in task-space \mathbf{f}_x and the joint control torques τ is given by

$$\tau = \mathbf{J}^T(\mathbf{q}) \mathbf{f}_x. \quad (3)$$

¹Property 1 is satisfied for robot manipulators with only revolute joints (Kelly *et al.*, 2005).

Then the model (1) can be rewritten in the task-space, using a coordinate change, as

$$\mathbf{M}_x \ddot{\mathbf{x}} + \mathbf{C}_x \dot{\mathbf{x}} + \mathbf{g}_x + \mathbf{F}_x \dot{\mathbf{x}} = \mathbf{f}_x - \mathbf{f}_e, \quad (4)$$

where $\mathbf{x} = \mathcal{K}(\mathbf{q}) \in \mathbb{R}^p$ is the task-space posture vector (forward kinematics map), $\dot{\mathbf{x}} = \mathbf{J}(\mathbf{q})\dot{\mathbf{q}} \in \mathbb{R}^p$ represents the task-space velocity, and $\ddot{\mathbf{x}} = \dot{\mathbf{J}}(\mathbf{q}, \dot{\mathbf{q}})\dot{\mathbf{q}} + \mathbf{J}(\mathbf{q})\ddot{\mathbf{q}} \in \mathbb{R}^p$ is the acceleration vector in task-space, while

$$\begin{aligned} \mathbf{M}_x &= \mathbf{J}^{-T}(\mathbf{q})\mathbf{M}(\mathbf{q})\mathbf{J}^{-1}(\mathbf{q}), \\ \mathbf{C}_x &= \left[\mathbf{J}^{-T}(\mathbf{q})\mathbf{C}(\mathbf{q}, \dot{\mathbf{q}}) - \mathbf{M}_x \dot{\mathbf{J}}(\mathbf{q}, \dot{\mathbf{q}}) \right] \mathbf{J}^{-1}(\mathbf{q}), \\ \mathbf{g}_x &= \mathbf{J}^{-T}(\mathbf{q})\mathbf{g}(\mathbf{q}), \\ \mathbf{F}_x &= \mathbf{J}^{-T}(\mathbf{q})\mathbf{F}\mathbf{J}^{-1}(\mathbf{q}), \end{aligned}$$

where $\mathbf{J}^{-T}(\mathbf{q}) = [\mathbf{J}^{-1}(\mathbf{q})]^T$. The Cartesian dynamic model (4) is valid only if the manipulator is away from kinematic singularities, i.e., $\text{rank}(\mathbf{J}(\mathbf{q})) = n$, and this is a condition of operation of the proposed scheme. If the manipulator is redundant, i.e., $\mathbf{J}(\mathbf{q})$ is non-square, then a right pseudoinverse of the form

$$\mathbf{J}^\dagger = \mathbf{J}^T(\mathbf{q})[\mathbf{J}(\mathbf{q})\mathbf{J}^T(\mathbf{q})]^{-1} \quad (5)$$

can be computed instead (Canudas *et al.*, 2012). When $\mathbf{J}(\mathbf{q})$ is square, the pseudoinverse (5) is reduced to the standard inverse of the Jacobian matrix, $\mathbf{J}^{-1}(\mathbf{q})$. With no loss of generality, in this paper a square Jacobian matrix is considered, i.e., $p = n$.

Also, suppose that each component of vector \mathbf{f}_x is constrained by a saturation bound $F_{xj} > 0$; that is, $|f_{xj}| \leq F_{xj}$, with $j = 1, \dots, p$. Then, if u_{xj} represents the control signal to the j -th degree of freedom, we have the following relationship:

$$f_{xj} = F_{xj} \text{sat} \left(\frac{u_{xj}}{F_{xj}} \right). \quad (6)$$

Therefore, from (2)–(3) and (6),

$$\mathbf{u} = \mathbf{J}^T(\mathbf{q}) \mathbf{u}_x. \quad (7)$$

The vector of external forces is modeled as a generalized spring with symmetric stiffness matrix $\mathbf{K}_e \in \mathbb{R}^{p \times p}$ and rest location $\mathbf{x}_e \in \mathbb{R}^p$, i.e.,

$$\mathbf{f}_e = \mathbf{K}_e[\mathbf{x} - \mathbf{x}_e]. \quad (8)$$

The task-space dynamical model (4) has the following properties (Chávez-Olivares *et al.*, 2015).

Property 3. The matrix $\mathbf{M}_x \in \mathbb{R}^{p \times p}$ is symmetric and positive definite, and satisfies

$$\mu_m \mathbf{I}^p \leq \mathbf{M}_x \leq \mu_M \mathbf{I}^p$$

for some constants $\mu_M \geq \mu_m > 0$.

Property 4. The matrices $\dot{\mathbf{M}}_x \triangleq \frac{d}{dt} \mathbf{M}_x$ and $\mathbf{C}_x \in \mathbb{R}^{p \times p}$ satisfy

$$\dot{\mathbf{x}}^T \left[\frac{1}{2} \dot{\mathbf{M}}_x - \mathbf{C}_x \right] \dot{\mathbf{x}} = 0, \quad \forall \dot{\mathbf{x}} \in \mathbb{R}^p.$$

Property 5. The viscous friction matrix $\mathbf{F}_x \in \mathbb{R}^{p \times p}$ satisfies

$$f_m \mathbf{I}^p \leq \mathbf{F}_x \leq f_M \mathbf{I}^p$$

for some constants $f_M \geq f_m > 0$.

Property 6. The matrix $\mathbf{K}_e \in \mathbb{R}^{p \times p}$ is symmetric and positive definite and satisfies

$$k_m \mathbf{I}^p \leq \mathbf{K}_e \leq k_M \mathbf{I}^p$$

for some constants $k_M \geq k_m > 0$.

4. Saturating PD-type stiffness control for interaction tasks

The saturating stiffness controller is given by

$$\mathbf{u}_x(\mathbf{x}, \dot{\mathbf{x}}, \mathbf{q}) = -\mathbf{s}_d(\bar{\mathbf{x}}, \dot{\mathbf{x}}) - \mathbf{s}_P(\mathbf{K}_P \bar{\mathbf{x}}) + \mathbf{g}_x, \quad (9)$$

where $\bar{\mathbf{x}} = \mathbf{x} - \mathbf{x}_d$ for any constant, desired equilibrium position, $\mathbf{x}_d \in \mathbb{R}^p$, \mathbf{g}_x is the gravity compensation vector, $\mathbf{K}_P \in \mathbb{R}^{p \times p}$ is a positive definite diagonal matrix, i.e., $\mathbf{K}_P = \text{diag}[k_{P1}, \dots, k_{Pp}]$ with $k_{Pj} > 0$ for all $j = 1, \dots, p$,

$$\mathbf{s}_P : \begin{cases} \mathbb{R}^p \rightarrow \mathbb{R}^p, \\ \mathbf{x} \mapsto (\sigma_{P1}(x_1), \dots, \sigma_{Pp}(x_p))^T, \end{cases} \quad (10)$$

with $\sigma_{Pj}(\cdot)$, $j = 1, \dots, p$, being strictly increasing generalized saturation functions with bounds M_{Pj} , and $\mathbf{s}_d : \mathbb{R}^p \times \mathbb{R}^p \rightarrow \mathbb{R}^p$ a continuous vector function, which is bounded and satisfies

$$\mathbf{s}_d(\mathbf{y}, \mathbf{0}^p) = \mathbf{0}^p, \quad (11)$$

$$\|\mathbf{s}_d(\mathbf{y}, \mathbf{z})\| \leq \kappa \|\mathbf{z}\|, \quad (12)$$

$$\mathbf{z}^T \mathbf{s}_d(\mathbf{y}, \mathbf{z}) > 0, \quad (13)$$

$\forall \mathbf{y}, \mathbf{z} \in \mathbb{R}^p$, for some positive constant κ (Mendoza *et al.*, 2015a). Then, for suitable bounds M_{Pj} of $\sigma_{Pj}(\cdot)$,

$$|u_{xj}(\mathbf{y}, \mathbf{z})| < F_{xj}, \quad j = 1, \dots, p. \quad (14)$$

Property 7. Let $\mathbf{u}_x = \mathbf{u}_{PD} + \mathbf{g}_x$, with

$$\mathbf{u}_{PD} = -\mathbf{s}_d(\bar{\mathbf{x}}, \dot{\mathbf{x}}) - \mathbf{s}_P(\mathbf{K}_P \bar{\mathbf{x}}) \quad (15)$$

being the corresponding proportional-derivative action of the controller (9). Then, from (7), we have

$$|u_i| = |\mathbf{J}_i^T(\mathbf{q}) \mathbf{u}_x| = |\mathbf{J}_i^T(\mathbf{q}) \mathbf{u}_{PD} + g_i(\mathbf{q})| < T_i. \quad (16)$$

Notice that from (16) and (2) we get

$$T_i > |u_i(\mathbf{x}, \dot{\mathbf{x}}, \mathbf{q})| = |\tau_i|, \quad i = 1, \dots, n,$$

for all $(\mathbf{x}, \dot{\mathbf{x}}, \mathbf{q}) \in \mathbb{R}^p \times \mathbb{R}^p \times \mathbb{R}^n$. Then, along the system trajectories,

$$|\tau_i(t)| = |u_i(t)| < T_i, \quad i = 1, \dots, n,$$

for all $t \geq 0$. This proves that, under the proposed design, the saturation limits T_i are never reached.

Property 8. Consider the product $\mathbf{J}^T(\mathbf{q})\mathbf{u}_{PD}$. Let $u_M > 0$ represent an upper bound of \mathbf{u}_{PD} such that $\|\mathbf{u}_{PD}\| \leq u_M$. Now, from (16) and Property 1,

$$|\mathbf{J}_i^T(\mathbf{q})\mathbf{u}_{PD} + g_i(\mathbf{q})| \leq |\mathbf{J}_i^T(\mathbf{q})\mathbf{u}_{PD}| + B_{gi}, \quad (17)$$

assuming that

$$|\mathbf{J}_i^T(\mathbf{q})\mathbf{u}_{PD}| \leq \|\mathbf{J}_i^T(\mathbf{q})\| \|\mathbf{u}_{PD}\| < T_i - B_{gi}. \quad (18)$$

Thus, from Property 2, a sufficient condition on u_M is given by

$$u_M = \min_i \left\{ \frac{T_i - B_{gi}}{B_{Ji}} \right\}, \quad (19)$$

$i = 1, \dots, n$.

Remark 1. Multiple control structures arise from the formulation presented here, since $s_d(\bar{\mathbf{x}}, \dot{\mathbf{x}})$ can be designed as follows (López-Araujo *et al.*, 2013a): Let $\mathbf{K}_D \in \mathbb{R}^{p \times p}$ be a positive definite diagonal matrix, i.e., $\mathbf{K}_D = \text{diag}[k_{D1}, \dots, k_{Dp}]$ with $k_{Dj} > 0$ for all $j = 1, \dots, p$. An SP-SD stiffness controller is retrieved from (9) by defining

$$s_d(\bar{\mathbf{x}}, \dot{\mathbf{x}}) = s_D(\mathbf{K}_D \dot{\mathbf{x}}), \quad (20)$$

where

$$s_D : \begin{cases} \mathbb{R}^p \rightarrow \mathbb{R}^p, \\ \mathbf{x} \mapsto (\sigma_{D1}(x_1), \dots, \sigma_{Dp}(x_p))^T, \end{cases} \quad (21)$$

with $\sigma_{Dj}(\cdot)$, $j = 1, \dots, p$, being generalized saturation functions with bounds M_{Dj} . M_{Pj} and M_{Dj} satisfy

$$\sqrt{\sum_{j=1}^p [M_{Pj} + M_{Dj}]^2} < u_M. \quad (22)$$

Also, an SPD stiffness controller can be obtained by defining

$$s_d(\bar{\mathbf{x}}, \dot{\mathbf{x}}) = s_P(\mathbf{K}_P \bar{\mathbf{x}} + \mathbf{K}_D \dot{\mathbf{x}}) - s_P(\mathbf{K}_P \bar{\mathbf{x}}), \quad (23)$$

with bounds M_{Pj} , of the strictly increasing generalized saturation functions $\sigma_{Pj}(\cdot)$, $j = 1, \dots, p$, satisfying

$$\sqrt{\sum_{j=1}^p M_{Pj}^2} < u_M. \quad (24)$$

Remark 2. Note that the fulfillment of the inequalities (22) and (24), with u_M chosen as (19), is not necessary but only sufficient for avoiding saturation. Hence, the proposed scheme permits successful implementations with values $(T_i - B_{gi})/B_{Ji}$ higher than u_M .

4.1. Closed-loop analysis. By considering the robot model (4) and the saturating PD-type stiffness controller (9), the closed-loop dynamics can be written as

$$\mathbf{M}_x \ddot{\mathbf{x}} + \mathbf{C}_x \dot{\mathbf{x}} + \mathbf{F}_x \dot{\mathbf{x}} = -s_d(\bar{\mathbf{x}}, \dot{\mathbf{x}}) - s_P(\mathbf{K}_P \bar{\mathbf{x}}) - \mathbf{f}_e. \quad (25)$$

Under stationary conditions ($\ddot{\mathbf{x}} = \dot{\mathbf{x}} = \mathbf{0}^p$), it can be obtained that

$$\mathbf{f}_e = -s_P(\mathbf{K}_P \bar{\mathbf{x}}). \quad (26)$$

Since $\sigma_{Pj}(\cdot)$, are strictly increasing, generalised saturation functions; there is an $\bar{\mathbf{x}}^*$ such that $\mathbf{f}_e = -s_P(\mathbf{K}_P \bar{\mathbf{x}}^*)$ or, equivalently,

$$\bar{x}_j^* = -\frac{1}{k_{Pj}} \sigma_{Pj}^{-1}(f_{ej}), \quad j = 1, \dots, p. \quad (27)$$

Therefore, the equilibrium point is

$$\begin{bmatrix} \bar{\mathbf{x}} \\ \dot{\mathbf{x}} \end{bmatrix} = \begin{bmatrix} \bar{\mathbf{x}}^* \\ \mathbf{0}^p \end{bmatrix}. \quad (28)$$

4.2. Lyapunov stability analysis. In order to analyze the stability of the equilibrium point, the following scalar function is defined:

$$V(\bar{\mathbf{x}}, \dot{\mathbf{x}}) = \frac{1}{2} \dot{\mathbf{x}}^T \mathbf{M}_x \dot{\mathbf{x}} + \int_0^{\bar{\mathbf{x}}} s_P^T(\mathbf{K}_P r) dr + \frac{1}{2} [\mathbf{x} - \mathbf{x}_e]^T \mathbf{K}_e [\mathbf{x} - \mathbf{x}_e] - V_0, \quad (29)$$

where

$$V_0 = \int_0^{\bar{\mathbf{x}}^*} s_P^T(\mathbf{K}_P r) dr + \frac{1}{2} [\bar{\mathbf{x}}^* + \mathbf{x}_d - \mathbf{x}_e]^T \mathbf{K}_e [\bar{\mathbf{x}}^* + \mathbf{x}_d - \mathbf{x}_e] - \int_0^{\bar{\mathbf{x}}^*} s_P^T(\mathbf{K}_P r) dr = \sum_{j=1}^p \int_0^{\bar{x}_j^*} \sigma_{Pj}(k_{Pj} r_j) dr_j.$$

From Properties 3 and 6, and the definition and the corresponding properties of a generalized saturation function, we have that

$$V(\bar{\mathbf{x}}, \dot{\mathbf{x}}) > 0. \quad (30)$$

Observe that $W(\mathbf{0}^p, \dot{\mathbf{x}}) \rightarrow \infty$ as $\|\dot{\mathbf{x}}\| \rightarrow \infty$, and $W(\bar{\mathbf{x}}, \mathbf{0}^p) \rightarrow \infty$ as $\|\bar{\mathbf{x}}\| \rightarrow \infty$. Thus, $V(\bar{\mathbf{x}}, \dot{\mathbf{x}})$ is concluded to be positive definite and radially unbounded.

The derivative of the Lyapunov function (29), along the trajectories of the closed-loop system (25) with \mathbf{f}_e

defined as (8), is given as follows:

$$\begin{aligned}
 \dot{V}(\bar{\mathbf{x}}, \dot{\mathbf{x}}) &= \dot{\mathbf{x}}^T \mathbf{M}_x \ddot{\mathbf{x}} + \frac{1}{2} \dot{\mathbf{x}}^T \dot{\mathbf{M}}_x \dot{\mathbf{x}} + \mathbf{s}_P(\mathbf{K}_P \bar{\mathbf{x}})^T \dot{\mathbf{x}} \\
 &\quad + \dot{\mathbf{x}}^T \mathbf{K}_e [\mathbf{x} - \mathbf{x}_e] \\
 &= \dot{\mathbf{x}}^T [-\mathbf{s}_d(\bar{\mathbf{x}}, \dot{\mathbf{x}}) - \mathbf{s}_P(\mathbf{K}_P \bar{\mathbf{x}}) - \mathbf{K}_e [\mathbf{x} - \mathbf{x}_e] \\
 &\quad - \mathbf{C}_x \dot{\mathbf{x}} - \mathbf{F}_x \dot{\mathbf{x}}] + \frac{1}{2} \dot{\mathbf{x}}^T \dot{\mathbf{M}}_x \dot{\mathbf{x}} + \mathbf{s}_P^T(\mathbf{K}_P \bar{\mathbf{x}}) \dot{\mathbf{x}} \\
 &\quad + \dot{\mathbf{x}}^T \mathbf{K}_e [\mathbf{x} - \mathbf{x}_e] \\
 &= -\dot{\mathbf{x}}^T \mathbf{s}_d(\bar{\mathbf{x}}, \dot{\mathbf{x}}) + \dot{\mathbf{x}}^T \left[\frac{1}{2} \dot{\mathbf{M}}_x - \mathbf{C}_x \right] \dot{\mathbf{x}} \\
 &\quad - \dot{\mathbf{x}}^T \mathbf{F}_x \dot{\mathbf{x}} \\
 &= -\dot{\mathbf{x}}^T \mathbf{s}_d(\bar{\mathbf{x}}, \dot{\mathbf{x}}) - \dot{\mathbf{x}}^T \mathbf{F}_x \dot{\mathbf{x}}. \tag{31}
 \end{aligned}$$

Therefore, from Properties 4 and 5 as well as $\mathbf{s}_d(\bar{\mathbf{x}}, \dot{\mathbf{x}})$ satisfying (11) and (13), $\dot{V}(\bar{\mathbf{x}}, \dot{\mathbf{x}}) \leq 0$.

However, according to LaSalle's invariance principle (Khalil, 2002), consider the set

$$\begin{aligned}
 \Omega &= \{ \bar{\mathbf{x}}, \dot{\mathbf{x}} \in \mathbb{R}^p : \dot{V}(\bar{\mathbf{x}}, \dot{\mathbf{x}}) = 0 \} \\
 &= \{ \dot{\mathbf{x}} = \mathbf{0}^p, \bar{\mathbf{x}} \in \mathbb{R}^p \}. \tag{32}
 \end{aligned}$$

Then, $\dot{\mathbf{x}} \equiv \mathbf{0}^p \Rightarrow \ddot{\mathbf{x}} \equiv \mathbf{0}^p$, and from the closed-loop dynamics (4), $\dot{\mathbf{x}} \equiv \ddot{\mathbf{x}} \equiv \mathbf{0}^p \Rightarrow \mathbf{f}_e = -\mathbf{s}_P(\mathbf{K}_P \bar{\mathbf{x}}) \Rightarrow \bar{\mathbf{x}} = \bar{\mathbf{x}}^*$. Therefore, by invariance theory, the closed-loop equilibrium point $(\bar{\mathbf{x}}(t), \dot{\mathbf{x}}(t)) \equiv (\bar{\mathbf{x}}^*, \mathbf{0}^p)$ is concluded to be asymptotically stable.

5. Simulation results

In order to validate the efficiency of the proposed control scheme, three interaction tests were implemented using the model of two 3-DOF robot manipulators

5.1. Modeling robot manipulators. The first dynamic model corresponds to the anthropomorphic robot ROTRADI and was reported by Chávez-Olivares *et al.* (2012). According to the parameter values, Property 1 is satisfied with $B_{g1} = 0$, $B_{g2} = 57.7414$ Nm, and $B_{g3} = 2.1138$ Nm, while Property 2 with $B_{J1} = 0.9341$ m, $B_{J2} = 0.9$ m, and $B_{J3} = 0.45$ m. The maximum allowed torques (input saturation bounds) are $T_1 = 50$ Nm, $T_2 = 150$ Nm and $T_3 = 15$ Nm, respectively.

For comparison purposes, another robot with different dynamics was considered; thus, the second robot is a SCARA manipulator, and its dynamical model is characterized by

$$\mathbf{M}(\mathbf{q})\ddot{\mathbf{q}} + \mathbf{C}(\mathbf{q}, \dot{\mathbf{q}})\dot{\mathbf{q}} + \mathbf{f}(\dot{\mathbf{q}}) + \mathbf{g}(\mathbf{q}) = \boldsymbol{\tau} - \mathbf{J}^T(\mathbf{q})\mathbf{f}_e, \tag{33}$$

where

$$\begin{aligned}
 \mathbf{M}(\mathbf{q}) &= \begin{bmatrix} \theta_1 + 2\theta_2 \cos q_2 & \theta_3 + \theta_2 \cos q_2 & 0 \\ \theta_3 + \theta_2 \cos q_2 & \theta_3 & 0 \\ 0 & 0 & \theta_4 \end{bmatrix}, \\
 \mathbf{C}(\mathbf{q}, \dot{\mathbf{q}}) &= \begin{bmatrix} -\theta_2 \dot{q}_2 \sin q_2 & -\theta_2 (\dot{q}_1 + \dot{q}_2) \sin q_2 & 0 \\ \theta_2 \dot{q}_1 \sin q_2 & 0 & 0 \\ 0 & 0 & 0 \end{bmatrix}, \\
 \mathbf{f}(\dot{\mathbf{q}}) &= \begin{bmatrix} \theta_5 \dot{q}_1 + \theta_6 \text{sign } \dot{q}_1 \\ \theta_7 \dot{q}_2 + \theta_8 \text{sign } \dot{q}_2 \\ \theta_9 \dot{q}_3 + \theta_{10} \text{sign } \dot{q}_3 \end{bmatrix}, \\
 \mathbf{g}(\mathbf{q}) &= \begin{bmatrix} 0 \\ 0 \\ -9.81\theta_4 \end{bmatrix},
 \end{aligned}$$

with $\theta_1 = 2.8423$, $\theta_2 = 0.3195$, $\theta_3 = 0.3438$, $\theta_4 = 1.16$, $\theta_5 = 1.158$, $\theta_6 = 6.571$, $\theta_7 = 0.325$, $\theta_8 = 1.008$, $\theta_9 = 0.2$, $\theta_{10} = 0.7$ and

$$\mathbf{J}(\mathbf{q}) = \begin{bmatrix} -0.45 \sin q_1 - 0.45 \sin (q_1 + q_2) & J_{12} & 0 \\ 0.45 \cos q_1 + 0.45 \cos (q_1 + q_2) & J_{22} & 0 \\ 0 & 0 & -1 \end{bmatrix},$$

where

$$\begin{aligned}
 J_{12} &= -0.45 \sin (q_1 + q_2), \\
 J_{22} &= 0.45 \cos (q_1 + q_2).
 \end{aligned}$$

Therefore, Property 1 is satisfied with $B_{g1} = 0$, $B_{g2} = 0$, and $B_{g3} = 11.3796$ Nm, while Property 2 with $B_{J1} = 0.9$ m, $B_{J2} = 0.45$ m, and $B_{J3} = 1.0$ m. The maximum allowed input saturation bounds are $T_1 = 150$ Nm, $T_2 = 15$ Nm and $T_3 = 130$ N, respectively.

5.2. Interaction tests. The proposed controller (9) was tested in its SP-SD form, under the respective consideration of (22), with

$$\sigma_{Pj}(\zeta) = \begin{cases} \zeta, & |\zeta| \leq L_{Pj}, \\ \rho_{Pj}(\zeta), & |\zeta| > L_{Pj}, \end{cases} \tag{34}$$

$$\sigma_{Dj}(\zeta) = M_{Dj} \text{sat}(\zeta/M_{Dj}), \tag{35}$$

where

$$\begin{aligned}
 \rho_{Pj}(\zeta) &= \text{sign}(\zeta)L_{Pj} \\
 &\quad + (M_{Pj} - L_{Pj}) \tanh \left(\frac{\zeta - \text{sign}(\zeta)L_{Pj}}{M_{Pj} - L_{Pj}} \right),
 \end{aligned}$$

$j = 1, 2, 3$, with $0 < L_{Pj} < M_{Pj}$. Therefore, $\sigma'_{DjM} = 1$, $\forall j \in \{1, 2, 3\}$, and the inequality (12) is satisfied with $\kappa = \max_j \{k_{Dj}\}$.

For the controller's performance evaluation, three cases were considered and referred to as Tests 1, 2, and 3, respectively.

5.2.1. Test 1: Regulation to a single point. Test 1 consisted in getting that the robot's end effector interacts with a rigid flat surface (stiffness of 10000 N/m) inclined at 20 degrees to the horizontal and located inside the robot's task-space. The desired and initial conditions for the end-effector were (0.2881, 0.4483, -0.4755) m and (0.2881, 0.4248, -0.4108) m, respectively.

First, the anthropomorphic robot was considered; the corresponding initial joint position was $\mathbf{q}(0) = [-5, 95, -95]^T$ degrees and the saturation parameters of the controller were selected as $M_{P1} = 25$, $M_{P2} = 20$, $M_{P3} = 63.5$, $M_{D1} = 3$, $M_{D2} = 3$, $M_{D3} = 32$, and $L_{Pj} = 0.9M_{Pj}$, $j = 1, 2, 3$, while the control gains were chosen as: $\mathbf{K}_P = \text{diag}[1550, 1550, 1250]$ N/m and $\mathbf{K}_D = \text{diag}[100, 100, 370]$ N s/m. Figures 1–3 show the results for the anthropomorphic manipulator in Test 1. In Fig. 1, we show the positioning errors in the x , y and z directions.² Before the robot contacts the surface, the error components tend to zero, whereas when the robot's end effector interacts with the surface, a normal contact force is generated; then, the position error is different than zero, which is a desired feature. However, in Fig. 2, it can be observed that the steady-state force error tends to zero during robot–environment interaction. Furthermore, note that, from the graphs in Fig. 3, the control objective is achieved, avoiding input saturation.

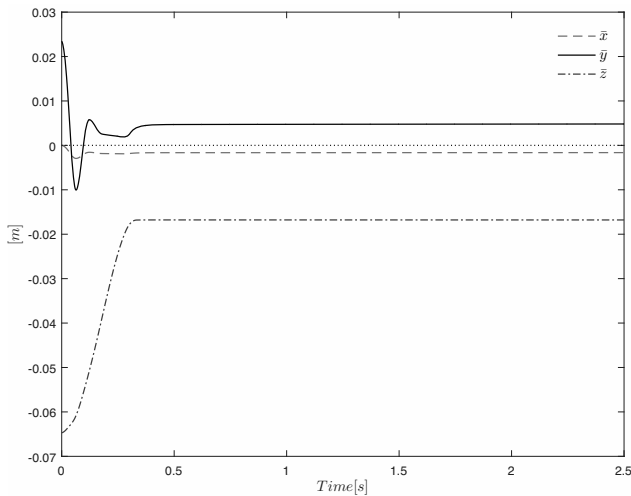


Fig. 1. Test 1: position errors in the task-space (anthropomorphic robot).

Then, the SCARA manipulator was used; the corresponding initial joint position was $\mathbf{q}(0) = [111.08, -110.46, 0.56]^T$ and the parameters of the SP-SD controller were $M_{P1} = 25$, $M_{P2} = 20$, $M_{P3} = 63.5$, $M_{D1} = 3$, $M_{D2} = 3$, $M_{D3} = 32$, and $L_{Pj} = 0.9M_{Pj}$, $j = 1, 2, 3$, while, $\mathbf{K}_P = \text{diag}[750, 750, 700]$

²In the notation used here the axes x , y and z correspond to x_1 , x_2 and x_3 , respectively; i.e., $\mathbf{x} = [x_1, x_2, x_3]^T$.

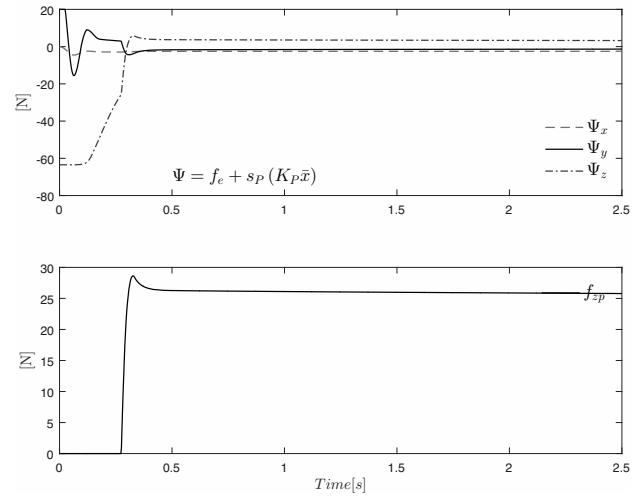


Fig. 2. Test 1: force error components and the normal interaction force (anthropomorphic robot).

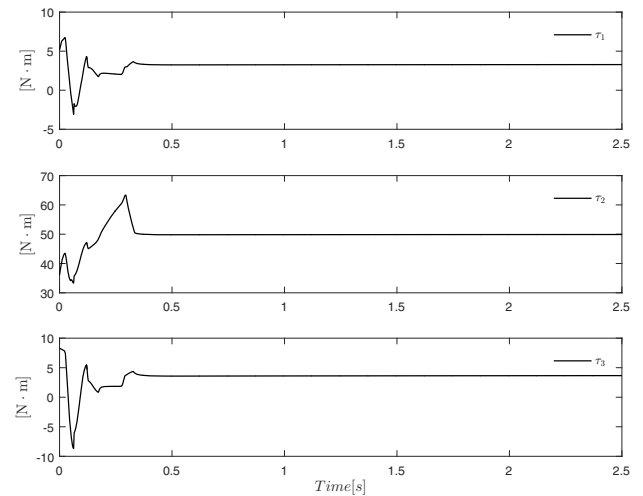


Fig. 3. Test 1: control torques applied (anthropomorphic robot).

and $\mathbf{K}_D = \text{diag}[150, 150, 1900]$. In Fig. 4, we can see smaller positioning errors in the x and y directions; this is because the structure of the SCARA configuration makes the interaction force mainly reflected in the z -axis direction. In Fig. 5, a steady-state force error close to zero and the corresponding normal interaction force can be observed. Also, input saturation is avoided as shown in Fig. 6.

5.2.2. Test 2: Tracking a point-to-point trajectory.

On the other hand, Test 2 consisted in making the robot's end-effector track a predefined point-to-point path over the same rigid flat surface, but now no inclination was considered. For both manipulators, the same saturation parameters used in Test 1 were assumed. In the case of the controller gains, only the proportional gains of

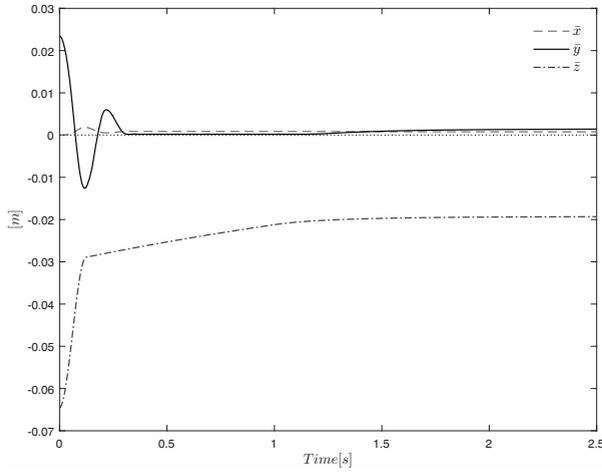


Fig. 4. Test 1: position errors in the task-space (SCARA robot).

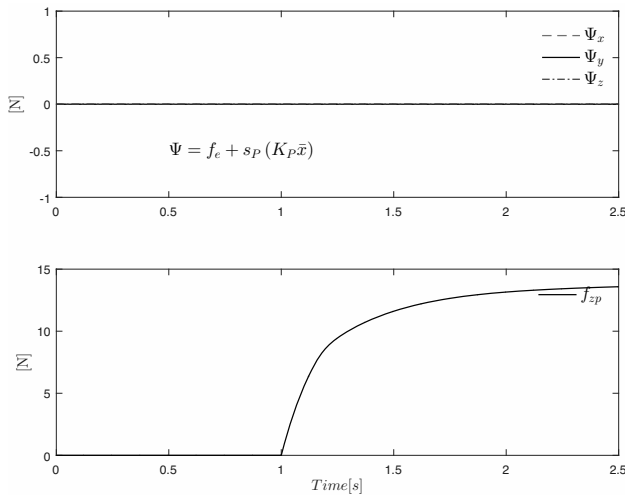


Fig. 5. Test 1: force error components and the normal interaction force (SCARA robot).

the ROTRADI robot were modified so that $\mathbf{K}_P = \text{diag}[10550, 10550, 1250]$ N/m. The path planning was as follows:

1. The robot must reach the position (0.2881, 0.4248, -0.5000) m, starting from the initial condition (0.2881, 0.4248, -0.4108) m in 1 seconds.
2. Using a linear interpolator, the robot must arrive at the position (0.3181, 0.3248, -0.5000) m in 5 seconds.
3. Using a linear interpolator, the robot must get to the position (0.3481, 0.4248, -0.5000) m in 5 seconds.

The corresponding desired path and the trajectory followed by the anthropomorphic and SCARA robots are depicted in Figs. 7 and 8, respectively. The positioning errors, for the ROTRADI robot, are presented in Fig. 9,

and it shows a suitable performance, with the components x and y tending to zero, and the z component tending to the difference between z_d and z_e . Therefore, it is ensured that the end effector is in contact with the surface and the interaction forces are being regulated. Finally, in Fig. 10, the control signals applied to the joints of the robot manipulator are presented. Because none of the components τ_i exceeds the corresponding torque limits T_i , it can be concluded that the task is performed without saturation of the system inputs.

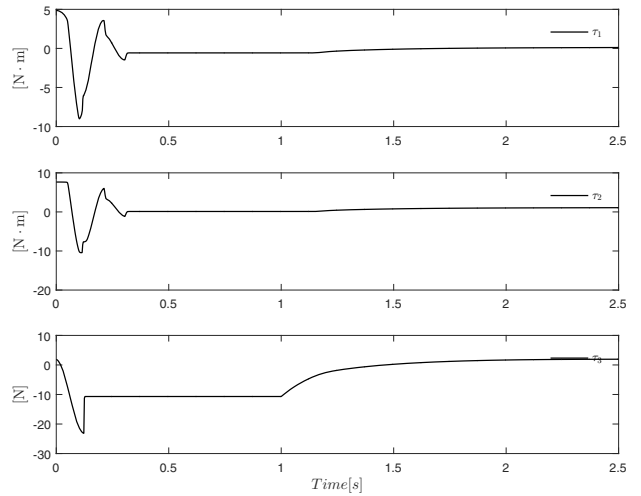


Fig. 6. Test 1: control torques/forces applied (SCARA robot).

5.2.3. Test 3: Robustness of the control scheme. In the last validation test, the proper controller performance was examined considering two scenarios: (a) the robot's behavior close to a singularity and (b) the operation of the control algorithm for inputs with smaller bounds. The ROTRADI robot was considered in Test 3.

In Test 3a, the robot tries to track the same path described in Test 2, but starting close to a singular configuration ($\mathbf{q}(0) = [-5, 55, -85]^T$ degrees), as can be seen in Fig. 11, where the singularities are defined by the points that are on the plane q_2-q_3 and for which $|\det(\mathbf{J}(\mathbf{q}))| = 0$; for example, $\mathbf{q} = [-5, 45, -90]^T$ implies $\det(\mathbf{J}(\mathbf{q})) = 0$ so we get a singularity.

As can be observed in Fig. 12, the effect of singularity is mainly reflected in the x component of the position error. However, the control signals remains bounded, as seen in Fig. 13. Then, the robot tries to follow the path in contact with the surface and without saturation of the system inputs.

In Test 3b, on the other hand, the maximum torque for the second joint of the ROTRADI robot was considered as $T_2 = 125$ Nm, since the tracking task was more demanding. According to Remark 2, a suitable tuning of the controller parameters can be obtained by

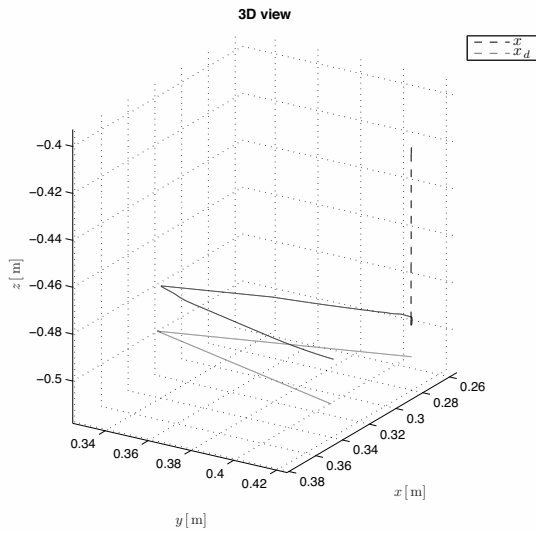


Fig. 7. Test 2: path tracking (anthropomorphic robot).

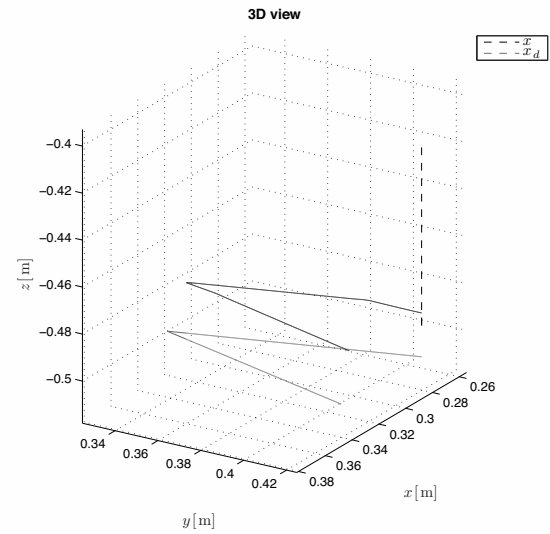


Fig. 8. Test 2: path tracking (SCARA robot).

computing $(T_2 - B_{g2})/B_{J2}$; therefore, the higher value in Test 2 was 102.51 while in Test 3b it was 74.73, and this restricts further selection of M_{Pj} and M_{Dj} . Then the new controller parameters were $M_{P1} = 21$, $M_{P2} = 19$, $M_{P3} = 42$, $M_{D1} = 3$, $M_{D2} = 3$, $M_{D3} = 25$, and $L_{Pj} = 0.9M_{Pj}$, $j = 1, 2, 3$, while, the control gains were chosen as $\mathbf{K}_P = \text{diag}[10550, 15550, 1350]$ N/m and $\mathbf{K}_D = \text{diag}[100, 100, 370]$ N s/m.

Despite the additional constraints, the robot's behavior is very similar to that obtained in Test 2 (see Figs. 9 and 10) and this can be observed in Figs. 14 and 15. Therefore, a suitable path tracking in contact with the surface is achieved and no saturation is presented.

6. Conclusions

In this paper, a generalized PD-type stiffness control scheme for robot manipulators with bounded inputs has been presented. To our knowledge, the saturating structure of this approach represents a first step in addressing the problem of controlling the robot–environment interaction, by considering the effect of saturation of the actuators of a robot manipulator.

The suitable performance of the control scheme was supported by a stability analysis in the Lyapunov sense, and its efficiency was verified through implementations on two 3-DOF robot manipulators. Moreover, the proposed scheme uses generalized saturation functions to achieve the required boundedness, which include the hyperbolic tangent and the conventional saturation as particular cases, and give rise to multiple particular PD-type stiffness controllers, permitting further innovation in their design and a wide range of possibilities for performance improvement.

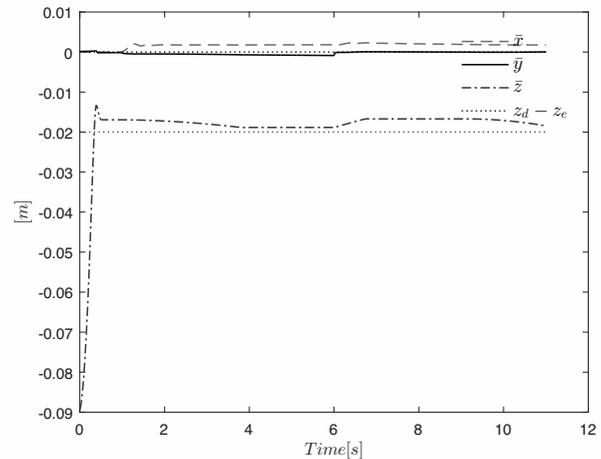


Fig. 9. Test 2: position errors in the task-space (anthropomorphic robot).

Acknowledgment

The authors wish to thank CONACYT for the support provided through the project no. 222316.

References

- Aguiñaga-Ruiz, E., Zavala-Río, A., Santibáñez, V. and Reyes, F. (2009). Global trajectory tracking through static feedback for robot manipulators with bounded inputs, *IEEE Transactions on Control Systems Technology* **17**(4): 934–944.
- Akdoğan, E. and Adli, M.A. (2011). The design and control of a therapeutic exercise robot for lower limb rehabilitation: Physiotherobot, *Mechatronics* **21**(3): 509–522.
- Belter, D., Łabecki, P., Fankhauser, P. and Siegart, R. (2016). RGB-D terrain perception and dense mapping

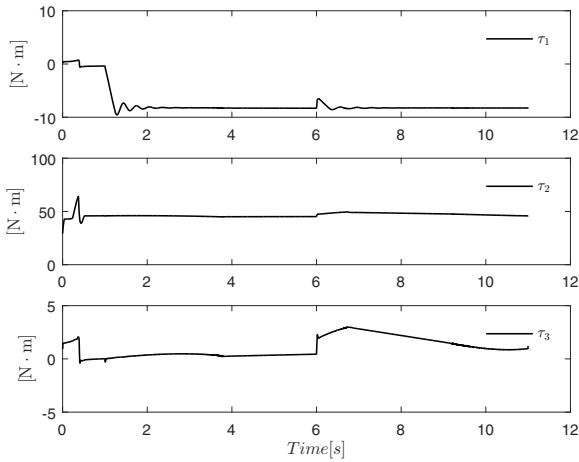


Fig. 10. Test 2: control torques applied (anthropomorphic robot).

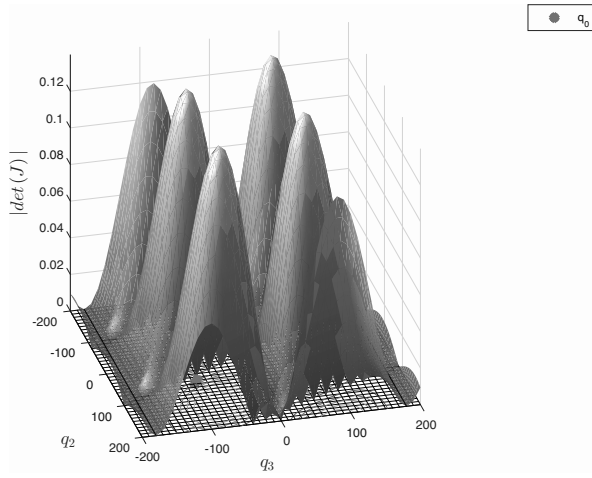


Fig. 11. Test 3a: singularity of the anthropomorphic robot.

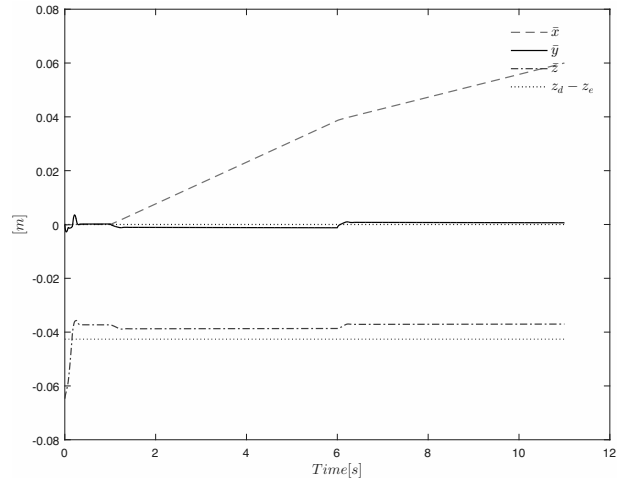


Fig. 12. Test 3a: position errors in the task-space (anthropomorphic robot).

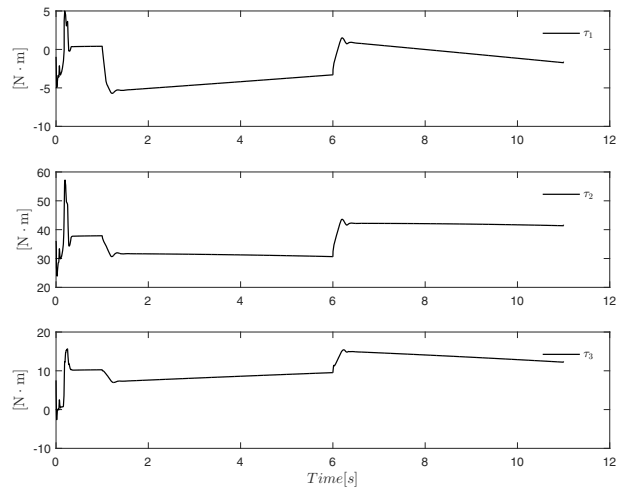


Fig. 13. Test 3a: control torques applied (anthropomorphic robot).

for legged robots, *International Journal of Applied Mathematics and Computer Science* **26**(1): 81–97, DOI: 10.1515/amcs-2016-0006.

Canudas, C., Siciliano, B. and Bastin, G. (2012). *Theory of Robot Control*, Springer-Verlag, London.

Caverly, R.J., Zlotnik, D.E., Bridgeman, L.J. and Forbes, J.R. (2014). Saturated proportional derivative control of flexible-joint manipulators, *Robotics and Computer-Integrated Manufacturing* **30**(6): 658–666.

Caverly, R.J., Zlotnik, D.E. and Forbes, J.R. (2016). Saturated control of flexible-joint manipulators using a Hammerstein strictly positive real compensator, *Robotica* **34**(06): 1367–1382.

Chávez-Olivares, C., Reyes, F. and González-Galván, E. (2015). On stiffness regulators with dissipative injection for robot manipulators, *International Journal of Advanced Robotic Systems* **12**(65): 1–15.

Chávez-Olivares, C., Reyes, F., González-Galván, E., Mendoza, M. and Bonilla, I. (2012). Experimental evaluation of

parameter identification schemes on an anthropomorphic direct drive robot, *International Journal of Advanced Robotic Systems* **9**(203): 1–18.

Dario, P., Guglielmelli, E. and Allotta, B. (1994). Robotics in medicine, *IEEE/RSJ/GI International Conference on Intelligent Robots and Systems: Advanced Robotic Systems and the Real World, IROS'94, Munich, Germany, Vol. 2*, pp. 739–752.

Dehghani, S., Taghirad, H. and Darainy, M. (2010). Self-tuning dynamic impedance control for human arm motion, *7th Iranian Conference of Biomedical Engineering (ICBME), Isfahan, Iran*, pp. 1–5.

Deneve, A., Moughamir, S., Afilal, L. and Zaytoon, J. (2008). Control system design of a 3-DOF upper limbs rehabilitation robot, *Computer Methods and Programs in Biomedicine* **89**(2): 202–214.

Djebrani, S., Benali, A. and Abdessemed, F. (2012). Modelling and control of an omnidirectional mobile

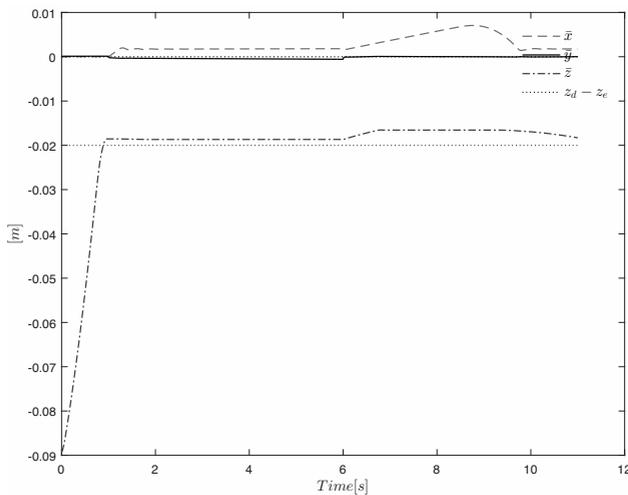


Fig. 14. Test 3b: position errors in the task-space (anthropomorphic robot).

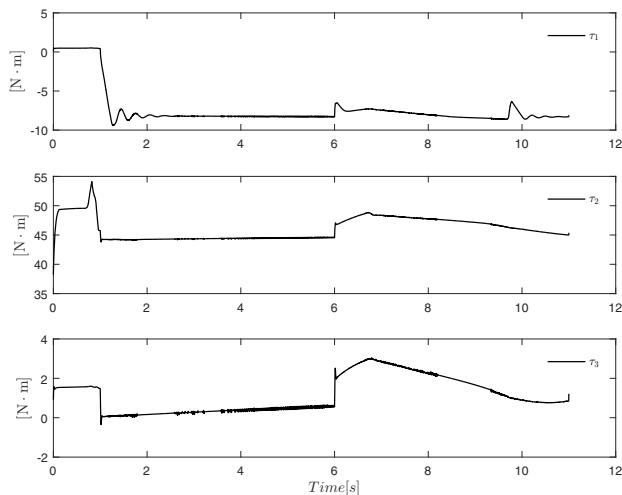


Fig. 15. Test 3b: control torques applied (anthropomorphic robot).

manipulator, *International Journal of Applied Mathematics and Computer Science* **22**(3): 601–616, DOI: 10.2478/v10006-012-0046-1.

Duleba, I. and Opałka, M. (2013). A comparison of Jacobian-based methods of inverse kinematics for serial robot manipulators, *International Journal of Applied Mathematics and Computer Science* **23**(2): 373–382, DOI: 10.2478/amcs-2013-0028.

Falaki, A. and Towhidkhan, F. (2012). Supervisory model predictive impedance control for human arm movement, *20th Iranian Conference on Electrical Engineering, Tehran, Iran*, pp. 1562–1566.

He, W., Dong, Y. and Sun, C. (2016). Adaptive neural impedance control of a robotic manipulator with input saturation, *IEEE Transactions on Systems, Man, and Cybernetics: Systems* **46**(3): 334–344.

Hogan, N. (1985). Impedance control: An approach to manipulation. I: Theory, II: Implementation, III: Applications, *ASME Journal of Dynamic Systems, Measurement and Control* **107**(1): 1–24.

Ju, M.S., Lin, C.C.K., Lin, D.H., Hwang, I.S. and Chen, S.M. (2005). A rehabilitation robot with force-position hybrid fuzzy controller: Hybrid fuzzy control of rehabilitation robot, *IEEE Transactions on Neural Systems & Rehabilitation Engineering* **13**(3): 349–358.

Kelly, R., Santibáñez, V. and Berghuis, H. (1997). Point-to-point robot control under actuator constraints, *Control Engineering Practice* **5**(11): 1555–1562.

Kelly, R., Santibáñez, V. and Loría, A. (2005). *Control of Robot Manipulators in Joint Space*, Springer-Verlag, London.

Khalil, H. (2002). *Nonlinear Systems*, Prentice Hall, Upper Saddle River, NJ.

Kiguchi, K., Imada, Y. and Liyanaje, M. (2007). EMG-based neuro-fuzzy control of a 4-DOF upper-limb power-assist exoskeleton, *29th Annual International Conference of the IEEE Engineering in Medicine and Biology Society, Lyon, France*, pp. 3040–3043.

Kurfess, T. (2004). *Robotics and Automation Handbook*, CRC Press, Boca Raton, FL.

Li, Y., Ge, S.S., Yang, C., Li, X. and Tee, K.P. (2011). Model-free impedance control for safe human–robot interaction, *2011 IEEE International Conference on Robotics and Automation (ICRA), Shanghai, China*, pp. 6021–6026.

López-Araujo, D.J., Zavala-Río, A., Santibáñez, V. and Reyes, F. (2013a). A generalized scheme for the global adaptive regulation of robot manipulators with bounded inputs, *Robotica* **31**(7): 1103–1117.

López-Araujo, D.J., Zavala-Río, A., Santibáñez, V. and Reyes, F. (2013b). Output-feedback adaptive control for the global regulation of robot manipulators with bounded inputs, *International Journal of Control, Automation, and Systems* **11**(1): 105–115.

López-Araujo, D. J., Zavala-Río, A., Santibáñez, V. and Reyes, F. (2015). A generalized global adaptive tracking control scheme for robot manipulators with bounded inputs, *International Journal of Adaptive Control and Signal Processing* **29**(2): 180–200.

Mendoza, M., Bonilla, I., Reyes, F. and González-Galván, E. (2012). A Lyapunov-based design tool of impedance controllers for robot manipulators, *Kybernetika* **48**(6): 1136–1155.

Mendoza, M., Zavala-Río, A., Santibáñez, V. and Reyes, F. (2015a). A generalised PID-type control scheme with simple for the global regulation of robot manipulators with tuning constrained inputs, *International Journal of Control* **88**(10): 1995–2012.

Mendoza, M., Zavala-Río, A., Santibáñez, V. and Reyes, F. (2015b). Output-feedback proportional-integral-derivative-type control with simple tuning for the global regulation of robot manipulators with input constraints, *IET Control Theory and Applications* **9**(14): 2097–2106.

- Modares, H., Ranatunga, I., Lewis, F.L. and Popa, D.O. (2016). Optimized assistive human–robot interaction using reinforcement learning, *IEEE Transactions on Cybernetics* **46**(3): 655–667.
- Santibáñez, V. and Kelly, R. (1996). Global regulation for robot manipulators under SP-SD feedback, *1996 IEEE International Conference on Robotics and Automation (ICRA), Minneapolis, MN, USA*, pp. 927–932.
- Santibáñez, V., Kelly, R. and Reyes, F. (1998). A new set-point controller with bounded torques for robot manipulators, *IEEE Transactions on Industrial Electronics* **45**(1): 126–133.
- Siciliano, B. and Villani, L. (2012). *Robot Force Control*, Springer-Verlag, London.
- Spong, M., Hutchinson, S. and Vidyasagar, M. (2005). *Robot Modeling and Control*, Wiley, New York, NY.
- Volpe, R. and Khosla, P. (1993). A theoretical and experimental investigation of explicit force control strategies for manipulators, *IEEE Transactions on Automatic Control* **38**(11): 1634–1650.
- Xu, G., Song, A. and Li, H. (2011). Adaptive impedance control for upper-limb rehabilitation robot using evolutionary dynamic recurrent fuzzy neural network, *Journal of Intelligent & Robotic Systems* **62**(3): 501–525.
- Yarza, A., Santibanez, V. and Moreno-Valenzuela, J. (2013). An adaptive output feedback motion tracking controller for robot manipulators: Uniform global asymptotic stability and experimentation, *International Journal of Applied Mathematics and Computer Science* **23**(3): 599–611, DOI: 10.2478/amcs-2013-0045.
- Zavala-Río, A. and Santibáñez, V. (2006). Simple extensions of the PD-with-gravity-compensation control law for robot manipulators with bounded inputs, *IEEE Transactions on Control Systems Technology* **14**(5): 958–965.
- Zavala-Río, A. and Santibáñez, V. (2007). A natural saturating extension of the PD-with-desired-gravity-compensation control law for robot manipulators with bounded inputs, *IEEE Transactions on Robotics* **23**(2): 386–391.



María del Carmen Rodríguez-Liñán received the BE degree in electronic engineering and the MSc degree in electrical engineering from the University of San Luis Potosí, Mexico, in 2006 and 2008, and the PhD degree in electrical and electronic engineering from the University of Manchester, UK, in 2013. From 2014 to 2016 she was a postdoctoral fellow at the Autonomous University of San Luis Potosí. She is currently a CONACYT research fellow commissioned to the Ensenada Institute of Technology, Mexico. Her research interests include nonlinear systems, hard nonlinearities and robot control.



Marco Mendoza received the BE degree in communications and electronics engineering from the University of Colima, Mexico, in 2003, the MSc degree in electronics from the Autonomous University of Puebla, Mexico, in 2006, and the PhD degree in electrical engineering from the Autonomous University of San Luis Potosí, Mexico, in 2011. He was an associate professor at the University of Sonora, Mexico, from 2011 to 2012. He joined the Autonomous University of San Luis Potosí, Mexico, in 2014, where he is presently a professor of biomedical engineering. His current research interests include robot control and biorobotics.



Isela Bonilla received the BE degree in communications and electronics engineering from the University of Colima, Mexico, in 2003, the MSc degree in electronics from the Autonomous University of Puebla, Mexico, in 2006, and the PhD degree in electrical engineering from the Autonomous University of San Luis Potosí, in 2011. She joined the Autonomous University of San Luis Potosí, Mexico, in 2012, where she is presently a professor of electronic engineering and instrumentation. Her current research interests include impedance/force control and rehabilitation robotics.



César A. Chávez-Olivares was born in Aguascalientes, Mexico, in 1983. He received the BE degree in electronic engineering from the Autonomous University of Aguascalientes, Mexico, in 2006, and the MEng and PhD degrees in electrical engineering from the Autonomous University of San Luis Potosí, Mexico, in 2009 and 2014, respectively. He was a CONACYT research fellow at the Aguascalientes Institute of Technology, Mexico, from 2014 to 2015. In 2015, he joined the Center of Engineering Sciences at the Autonomous University of Aguascalientes, where he is currently a professor and a researcher. His research interests include vision systems, modeling, identification, and control of robot manipulators.

Received: 9 June 2016

Revised: 7 November 2016

Accepted: 6 December 2016